Volume 45 | Number 42 | 14 November 2016 | Pages 16535–17054

Dalton Transactions

An international journal of inorganic chemistry

www.rsc.org/dalton

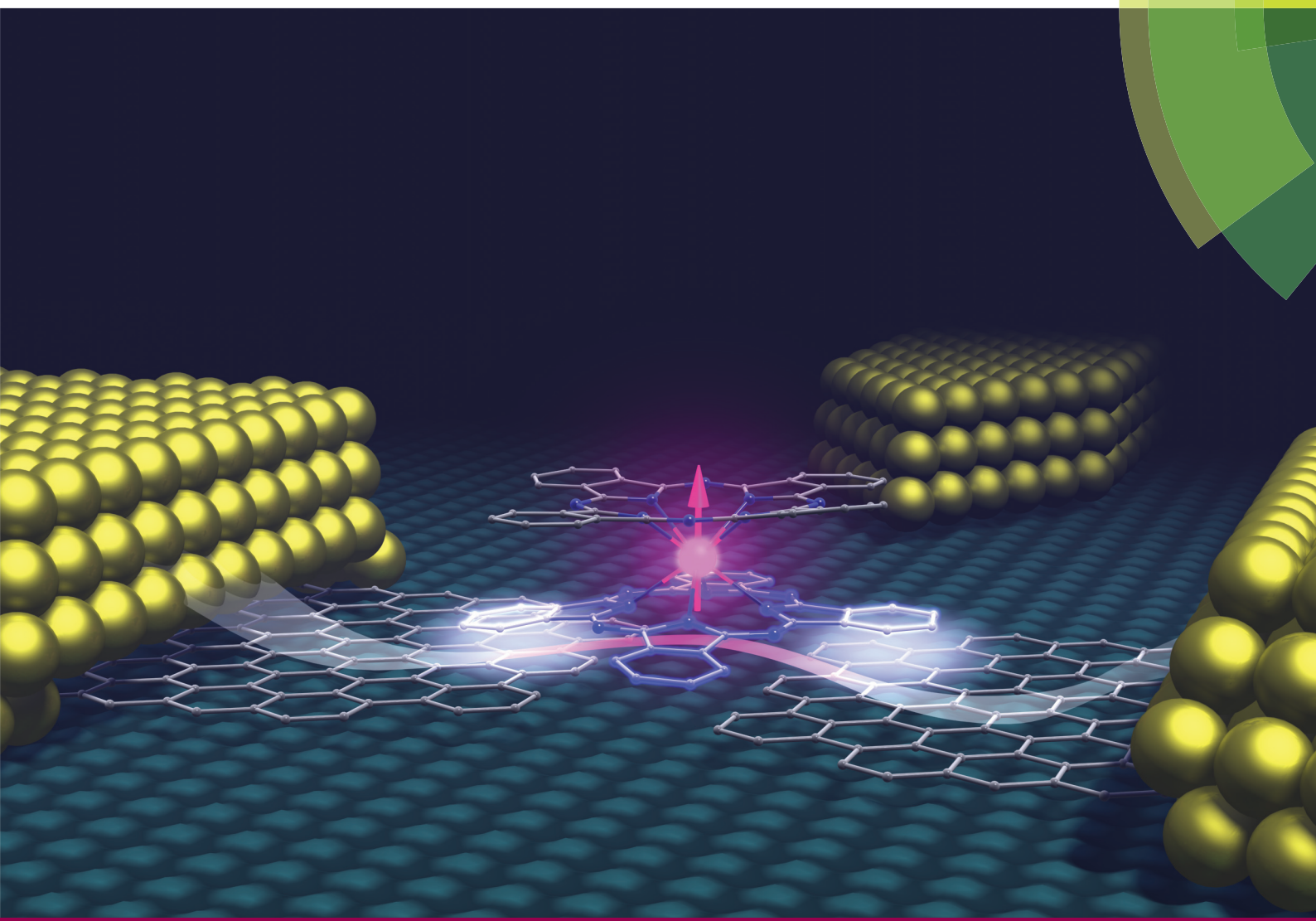

Featuring the themed issue: Molecular spintronics: the role of coordination chemistry

ISSN 1477-9226

ROYAL SOCIETY OF CHEMISTRY

COMMUNICATION
S. Lumetti *et al.*
Single-molecule devices with graphene electrodes

175 YEARS

Dalton Transactions

COMMUNICATION

View Article Online
View Journal | View Issue

Single-molecule devices with graphene electrodes

S. Lumetti,*[a,b] A. Candini,[a] C. Godfrin,[c,d] F. Balestro,[c,d,e] W. Wernsdorfer,[c,d] S. Klyatskaya,[f] M. Ruben[f,g] and M. Affronte[a,b]

Cite this: *Dalton Trans.*, 2016, **45**, 16570

Received 18th June 2016,
Accepted 11th August 2016

DOI: 10.1039/c6dt02445a

www.rsc.org/dalton

Several technological issues have to be faced to realize devices working at the single molecule level. One of the main challenges consists of defining methods to fabricate electrodes to make contact with single molecules. Here, we report the realization of novel spintronic devices made of a $TbPc_2$ single molecule embedded between two nanometer-separated graphene electrodes, obtained by feedback-controlled electroburning. We demonstrate that this approach allows the realisation of devices working at low temperature. With these, we were able to characterize the magnetic exchange coupling between the electronic spin of the Tb^{3+} magnetic core and the current passing through the molecular system in the Coulomb blockade regime, thus showing that the use of graphene is a promising way forward in addressing single molecules.

Introduction

Single-ion magnets are ideal candidates as building blocks for molecular spintronics, where both the electron charge and spin are exploited.[1,2] Even though great advances have been made in molecular (spin-)electronics over the past few decades, dealing with a single molecule still involves huge technological challenges. In particular, finding reliable methods to include single molecules in electronic circuits is a crucial issue to be solved to accomplish mass production of devices.[3] Several approaches have been proposed to realize molecular junctions, the most popular ones being mechanical break junctions,[4] electromigrated junctions[5] and scanning probe-based techniques.[6] Gold is traditionally used for the fabrication of such junctions as it is inert to most chemical environments and remains relatively easy to handle, though its high atomic mobility limits the mechanical stability of the resulting devices and their use for room-temperature applications.[3,7,8] An alternative strategy to fabricate stable molecular-scale electrodes is the use of graphene.[9–11] Its 2D fabric reduces the size mismatch between electrodes and molecules and its covalent bond-structure assures stability up to high temperatures. One of the most interesting features of graphene for molecular (spin-)electronics is the large spectrum of possibilities allowed for it to anchor diverse molecules covalently or using π–π stacking. Moreover, the energy gap between the chemical potential of the electrodes and the molecular electronic levels is expected to be reduced by carbon–carbon bonds, thus favouring charge injection.

Graphene can be produced on a large scale, which is an essential pre-requisite for the development of scalable complex architectures. Nonetheless, most of the methods conceived to prepare large area graphene, such as chemical vapour deposition[12,13] (CVD), are optimized to synthesize films of monolayer graphene, whose transport properties are strongly influenced by the application of a gate potential. In this regard, few-layer graphene seems to be a preferable choice for molecular electronics, since it displays a very small dependence on the gate voltage.[10,14] This kind of graphene can be obtained on large areas, for instance, by growing on the C-face of SiC.[15–18]

In this work, we report on the realization and the functional characterization of three-terminal molecular devices in which a bis(phthalocyanine) terbium(III) single-ion magnet ($TbPc_2$ hereafter) is embedded between two nano-gapped few-layer graphene electrodes obtained by electroburning (see Fig. 1). Thanks to its specific magnetic features (including a well-defined uniaxial anisotropy) and its robustness when deposited on a surface, the $TbPc_2$ single-ion magnet[19–21] is perfectly suited for the fabrication of a molecular spin transistor.[22,23]

[a]*Istituto Nanoscienze – CNR, Centro S3 Modena, via G. Campi 213A, 41124 Modena, Italy. E-mail: stefano.lumetti@unimore.it*
[b]*Dipartimento di Scienze Fisiche, Informatiche e Matematiche, Università degli Studi di Modena e Reggio Emilia, via G. Campi 213A, 41124 Modena, Italy*
[c]*Université Grenoble Alpes, Institut Néel, F-38042 Grenoble, France*
[d]*CNRS, Institut Néel, F-38042 Grenoble, France*
[e]*Institut Universitaire de France, 103 boulevard Saint-Michel, 75005 Paris, France*
[f]*Institute of Nanotechnology, Karlsruhe Institute of Technology (KIT), D-76344 Eggenstein-Leopoldshafen, Germany*
[g]*Institut de Physique et Chimie des Matériaux de Strasbourg, UMR 7504 UdS-CNRS, 67034 Strasbourg Cedex 2, France*

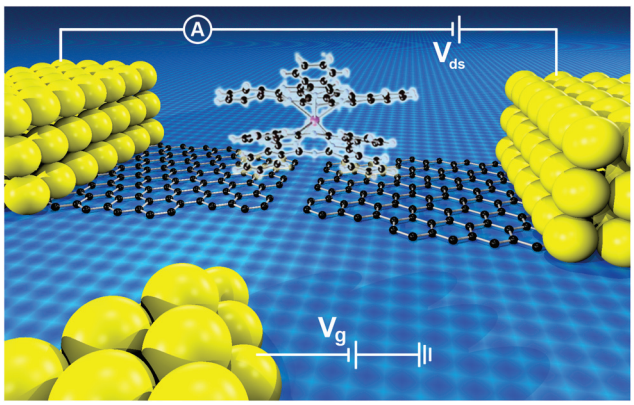

Fig. 1 Artist's impression of the molecular device with graphene electrodes and a $TbPc_2$ single-ion magnet located in the junction. A lateral gate electrode approaches the nanogap. The measurement set-up is also displayed in the schematics.

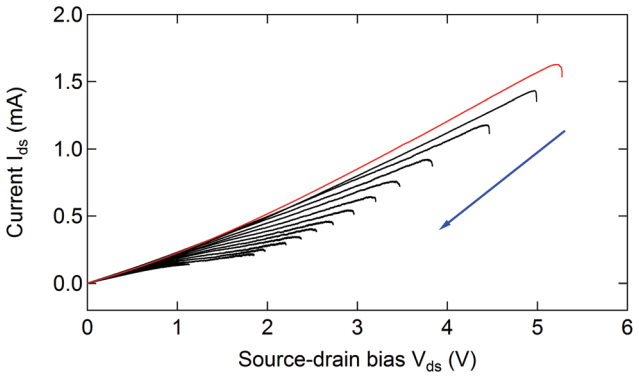

Fig. 2 Set of *I*–*V* characteristics showing the evolution (see blue arrow) of the feedback-controlled EB process. A voltage ramp is applied across the device until its resistance increases by more than a predefined percentage. The process is iterated until the low-bias resistance reaches 100 kΩ–4 MΩ.

Experimental

Few-layer graphene devices are fabricated on a SiC wafer following the methods reported in ref. 24. Afterwards, nanometer-sized gaps are opened in the resulting graphene junctions using a feedback-controlled electroburning (EB) procedure[10] that exploits the chemical reaction of carbon atoms with oxygen at high temperatures induced by Joule heating at large current densities. The presence of a fast feedback loop avoids the abrupt rupture of the graphene junctions and allows for a more accurate control on their final structure.

During the feedback-controlled EB, which is performed in air at room temperature, the source–drain voltage is swept across the graphene junction (at a rate between 50 and 100 mV s^{-1}) and the current flowing through the device is measured in a continuous manner in order to check the variations of the junction's low-bias resistance (R). An increase of R by more than a predefined percentage triggers the feedback control, which sweeps the voltage back to zero in 1 ms and starts a new voltage ramp immediately after, thereby iterating the same process until the low-bias resistance of the graphene device exceeds a predefined threshold value.

As depicted in Fig. 2, during the first voltage ramp the corresponding *I*–*V* curve (see red trace) usually displays a non-linear behaviour which is likely related to the removal of contaminants from the graphene surface caused by current annealing.[25,26] The downward curvature of the *I*–*V* characteristics marks the occurrence of the EB event. As the EB process moves forward, the device resistance increases in steps (indicating that the graphene junction is gradually narrowing down) and the voltage at which EB takes place progressively decreases (see the blue arrow in Fig. 2).

The EB procedure described above has a reasonable yield: out of 76 electroburnt junctions, 66 (87%) were controllably brought to a low-bias resistance in the range between 100 kΩ and 4 MΩ. In the other cases gaps with too high low-bias resistance (>1 GΩ) were created since the feedback loop did not respond fast enough.

The SEM image of a typical graphene device after EB is displayed in Fig. 3. A nm-sized gap can be seen in the central notched region of the junction. Indeed, during EB the highest temperature is reached in the middle patterned region (where the device cross section is the lowest) as a result of the Joule heating at large current densities: this, as well as the fact that the largest part of the heat is removed from the device by the metal electrodes, fosters the eventual breaking of graphene.

After the fabrication of graphene-based electrodes through EB, $TbPc_2$ single-molecule magnets are deposited on the samples by dropcasting from a solution where the molecules are dispersed in dichloromethane.

The devices are finally cooled down to ~80 mK inside a dilution fridge endowed with a home-made 2D vector magnet that allows for magnetic field sweep rates up to 0.2 T s^{-1}. Since the refrigerator can be manually rotated along one of the magnetic field coil axes, in principle it is possible to study with

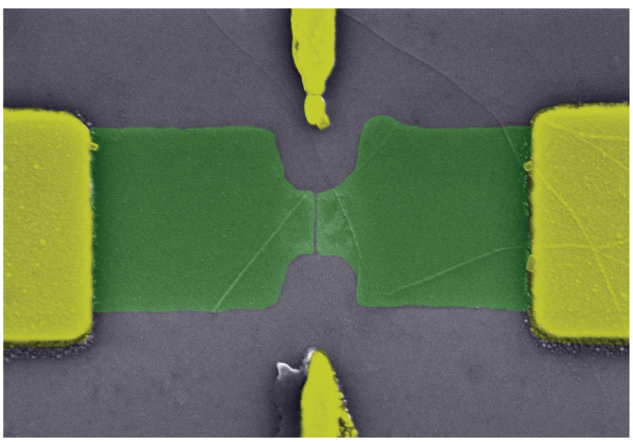

Fig. 3 False colour SEM image of a graphene junction after EB: a gap is visible in the centre of the middle "notched" region of the device.

this set-up the magnetic response of a physical system in three dimensions. Electrical transport measurements are performed using the lock-in technique with an AdWin-Pro system (16 bits output and 18 bits input) and a FEMTO pre-amplifier.

Results and discussion

Electrical transport measurements

The molecular devices are characterized by low-temperature electronic transport measurements. The differential conductance dI/dV of each device is measured as a function of the gate voltage V_g. Some of them display an insulating behaviour for the whole accessible gate range, except for one or few Coulomb peaks. These devices are further characterized by measuring their differential conductance as a function of both the source–drain voltage V_{ds} and the gate voltage V_g. Fig. 4 reports an example of one of the resulting stability diagrams, where the regions of high conductance are coloured in red and the regions of low conductance are coloured in blue. Two adjacent Coulomb diamonds can be identified along with several excited states that are clearly visible as multiple equidistant lines running parallel to the diamond's edges. Furthermore, inelastic cotunneling lines are found inside the diamond on the right side of the charge degeneracy point. This confirms that the charge transport through this device is in the Coulomb blockade regime and can be modelled by one or few quantum dots in parallel, supporting the picture that the current is flowing through one or few $TbPc_2$ molecules bridged between the graphene electrodes.

We have measured a total of 40 graphene nano-junctions functionalized with $TbPc_2$ molecules: 7 of them (17.5%) showed Coulomb blockade-like features, while other 26 (65%) either exhibited no dependence on the gate voltage (even though they displayed a measurable tunnelling current for $|V_{ds}| < 0.5$ V) or were in short circuit with one of the corresponding lateral gates. Finally, 7 devices (17.5%) were characterized by no tunnelling current for $|V_{ds}| < 1$ V (which is the signature of too large gaps between the graphene electrodes). Our yield is comparable to what has been reported in other studies on graphene-based molecular devices.[10,27–29]

Evidence of the molecule magnetism in the electrical transport

Previous reports on molecular transistors made by a single $TbPc_2$ molecule have demonstrated that the Pc ligands are tunnel-coupled to the source and drain terminals, thus creating a quantum dot in the vicinity of the electronic spin carried by the Tb^{3+} ion.[22,23] Moreover, it has been shown that the anisotropic magnetic moment of the Tb^{3+} ion is coupled with the organic ligands by an exchange interaction.[30] This causes the splitting of the energy levels of the molecular quantum dot.[22,23]

For one of our samples, we were able to estimate the nature and magnitude of this exchange coupling by measuring the differential conductance dI/dV as a function of the bias voltage V_{ds} and of the applied magnetic field B (see Fig. 5) near a charge degeneracy point. The measurements show that at a zero magnetic field the conductance is split into two resonances, whose energy separation decreases linearly with an increasing magnetic field, eventually leading to a single peak at $B_c \sim 1.4$ T. The slope obtained from the evolution of the two resonances is the signature of the spin-1/2 Kondo effect due to the presence of an unpaired electron in the quantum dot. The splitting of the Kondo peak at a zero magnetic field can be explained by accounting for an antiferromagnetic coupling with the Tb electronic spin, whose magnitude can be estimated from:[22]

$$a g_J \mu_B J_z = k_B T_K + 2 g \mu_B B_c$$

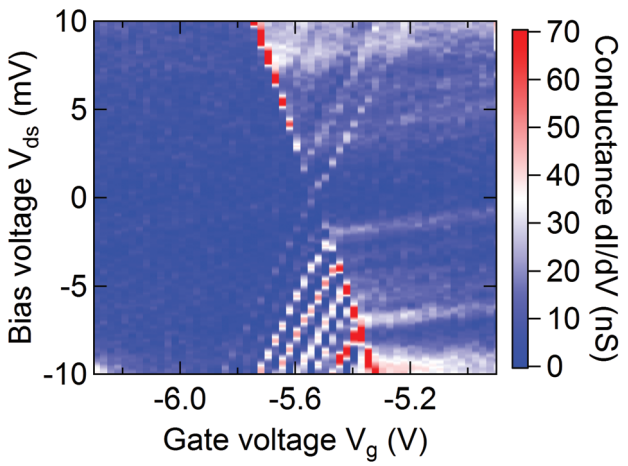

Fig. 4 Example of colour scale map of the differential conductance dI/dV as a function of gate voltage V_g and source–drain bias V_{ds}. The presence of characteristic Coulomb diamonds implies that the charge transport is in the Coulomb blockade regime. Several excited states are visible as well as inelastic cotunneling lines.

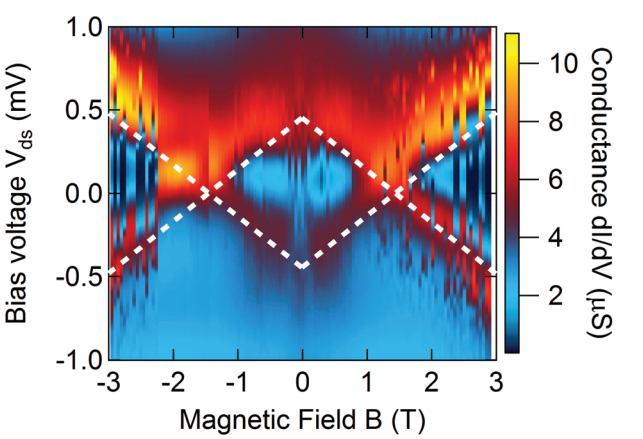

Fig. 5 Colour scale map of the differential conductance dI/dV measured as a function of the source–drain voltage V_{ds} and of the applied magnetic field B at a fixed gate potential. An antiferromagnetic exchange coupling between the current flowing through the molecular quantum dot and the Tb^{3+} electronic spin can be deduced, with a coupling constant $a \sim 1.10$ T.

where an exchange energy term $ag_J\mu_B J_z$ is included in the usual relationship describing the spin-1/2 Kondo effect. Here, a describes the magnitude of the interaction and it is defined as positive for an antiferromagnetic coupling, $g_J\mu_B J_z$ is the Tb magnetic moment (g_J = 1.5 being terbium's g-factor and μ_B the Bohr magneton), k_B the Boltzmann constant, T_K the Kondo temperature, g the g-factor for the electron in the dot and B_c the critical field inferred from the intersection of the Zeeman peaks at positive field values. The half width at half maximum (HWHM) of the Kondo signature at B_c = 1.4 T can be used to estimate the Kondo temperature through the approximate relationship[31] HWHM = $k_B T_K/e$. In our case HWHM ~ 250 μV, which yields $T_K \sim 2.9$ K. Therefore, a coupling constant $a \sim 1.10$ T can be extracted by inserting these values in the above equation. The efficient coupling between the two systems likely arises from the unbound electron of the Pc ligand with $S = 1/2$ which is close to the energy of the terbium 4f orbitals.[32] Moreover, such a high coupling between the quantum dot and the Tb^{3+} ion implies that these two systems are spatially very close, supporting once more the assumption that the quantum dot is created by the Pc ligands through which the electron transport takes place.

Conclusions

We have presented our recent results on the fabrication and test of novel molecular spin devices consisting of a $TbPc_2$ single-ion magnet embedded between two nanometer-separated graphene-based electrodes.

The opening of the nanogaps in the graphene junctions is made by means of a feedback-controlled electroburning technique carried out under ambient conditions. We showed that the EB process allows for a precise control over the structure of the graphene devices with a high rate of success. The molecule grafting on the graphene electrodes is still to be optimized, nonetheless we were able to derive an estimation of the strong exchange coupling between the Tb^{3+} electronic spin and the charge current flowing through the molecular quantum dot created by the organic ligands of the $TbPc_2$ single-ion magnet.

These preliminary results show that graphene is a suitable platform to make contact with single molecules and for the design of complex molecular-scale systems.

Acknowledgements

This work has been partially supported by the European Community through the FET-Proactive Project "*MoQuaS*", contract N. 610449, by the Italian Ministry for Research (MIUR) through the FIR grant RBFR13YKWX, and by the French Agency for Research through the ANR-12-JS10-007 SINUSManip and ANR-13-BS10-0001MolQuSpin projects. We thank E. Bonet (Institut Néel, Grenoble, France) for helping in software development, N. Mishra and C. Coletti (IIT Pisa, Italy) for providing the graphene substrates and P. Pingue and F. Carillo (Scuola Normale Superiore di Pisa, Italy) for assistance in sample fabrication and for the access to the nanofabrication facility of the Laboratorio NEST, Scuola Normale Superiore, Pisa, Italy.

Notes and references

1 D. Gatteschi, R. Sessoli and J. Villain, *Molecular Nanomagnets*, Oxford University Press, USA, 2006, ISBN 0198567537.
2 L. Bogani and W. Wernsdorfer, *Nat. Mater.*, 2008, **7**, 179.
3 E. Lörtscher, *Nat. Nanotechnol.*, 2013, **8**, 381.
4 M. A. Reed, C. Zhou, C. J. Muller, T. P. Burgin and J. M. Tour, *Science*, 1997, **278**, 252.
5 H. Park, A. K. L. Lim, A. P. Alivisatos, J. Park and P. L. McEuen, *Appl. Phys. Lett.*, 1999, **75**, 301.
6 L. A. Bumm, J. J. Arnold, M. T. Cygan, T. D. Dunbar, T. P. Burgin, T. P. Jones, D. L. Allara, J. M. Tour and P. S. Weiss, *Science*, 1996, **271**, 1705.
7 K. Moth-Poulsen and T. Bjørnholm, *Nat. Nanotechnol.*, 2009, **4**, 551.
8 M. Ratner, *Nat. Nanotechnol.*, 2013, **8**, 378.
9 L. Sun, Y. A. Diaz-Fernandez, T. A. Gschneidtner, F. Westerlund, S. Lara-Avila and K. Moth-Poulsen, *Chem. Soc. Rev.*, 2014, **43**, 7378.
10 F. Prins, A. Barreiro, J. W. Ruitenberg, J. S. Seldenthuis, N. Aliaga-Alcalde, L. M. K. Vandersypen and H. S. J. van der Zant, *Nano Lett.*, 2011, **11**, 4607.
11 Y. Cao, S. Dong, S. Liu, L. He, L. Gan, X. Yu, M. L. Steigerwald, X. Wu, Z. Liu and X. Guo, *Angew. Chem., Int. Ed.*, 2012, **51**, 12228.
12 K. S. Kim, Y. Zhao, H. Jang, S. Y. Lee, J. M. Kim, K. S. Kim, J.-H. Ahn, P. Kim, J.-Y. Choi and B. Hee, *Nature*, 2009, **457**, 706.
13 X. Li, W. Cai, J. An, S. Kim, J. Nah, D. Yang, R. Piner, A. Velamakanni, I. Jung, E. Tutuc, S. K. Banerjee, L. Colombo and R. S. Ruoff, *Science*, 2009, **324**, 1312.
14 E. Burzurí, F. Prins and H. S. J. van der Zant, *Graphene*, 2012, **1**, 26.
15 I. Forbeaux, J. M. Themlin and J. M. Debever, *Phys. Rev. B: Condens. Matter*, 1998, **58**, 16396.
16 C. Berger, Z. Song, T. Li, X. Li, A. Y. Ogbazghi, R. Feng, Z. Dai, A. N. Marchenkov, E. H. Conrad, P. N. First and W. A. de Heer, *J. Phys. Chem. B*, 2004, **108**, 19912.
17 T. Ohta, A. Bostwick, T. Seyller, K. Horn and E. Rotenberg, *Science*, 2006, **313**, 951.
18 C. Virojanadara, M. Syväjarvi, R. Yakimova, L. I. Johansson, A. A. Zakharov and T. Balasubramanian, *Phys. Rev. B: Condens. Matter*, 2008, **78**, 245403.
19 N. Ishikawa, M. Sugita, T. Okubo, N. Tanaka, T. Iino and Y. Kaizu, *Inorg. Chem.*, 2003, **42**, 2440.
20 P. Zhu, F. Lu, N. Pan, D. P. Arnold, S. Zhang and J. Jiang, *Eur. J. Inorg. Chem.*, 2004, **2004**, 510.
21 N. Ishikawa, M. Sugita and W. Wernsdorfer, *Angew. Chem., Int. Ed.*, 2005, **44**, 2931.

22 R. Vincent, S. Klyatskaya, M. Ruben, W. Wernsdorfer and F. Balestro, *Nature*, 2012, **488**, 357.
23 S. Thiele, F. Balestro, R. Ballou, S. Klyatskaya, M. Ruben and W. Wernsdorfer, *Science*, 2014, **344**, 1135.
24 A. Candini, N. Richter, D. Convertino, C. Coletti, F. Balestro, W. Wernsdorfer, M. Kläui and M. Affronte, *Beilstein J. Nanotechnol.*, 2015, **6**, 711.
25 J. Moser, A. Barreiro and A. Bachtold, *Appl. Phys. Lett.*, 2007, **91**, 163513.
26 C. Nef, L. Pósa, P. Makk, W. Fu, A. Halbritter, C. Schönenberger and C. Michel, *Nanoscale*, 2014, **6**, 7249.
27 J. A. Mol, C. S. Lau, W. J. M. Lewis, H. Sadeghi, C. Roche, A. Cnossen, J. H. Warner, C. J. Lambert, H. L. Anderson and G. A. D. Briggs, *Nanoscale*, 2015, **7**, 13181.
28 K. Ullmann, P. B. Coto, S. Leitherer, A. Molina-Ontoria, N. Martín, M. Thoss and H. B. Weber, *Nano Lett.*, 2015, **15**, 3512.
29 E. Burzurí, J. O. Island, R. Díaz-Torres, A. Fursina, A. González-Campo, O. Roubeau, S. J. Teat, N. Aliaga-Alcalde, E. Ruiz and H. S. J. van der Zant, *ACS Nano*, 2016, **10**, 2521.
30 A. Candini, D. Klar, S. Marocchi, V. Corradini, R. Biagi, V. De Renzi, U. del Pennino, F. Troiani, V. Bellini, S. Klyatskaya, M. Ruben, K. Kummer, N. B. Brookes, H. Huang, A. Soncini, H. Wende and M. Affronte, *Sci. Rep.*, 2016, **6**, 21740.
31 D. G. Scott and D. Natelson, *ACS Nano*, 2010, **4**, 3560.
32 L. Vitali, S. Fabris, A. M. Conte, S. Brink, M. Ruben, S. Baroni and K. Kern, *Nano Lett.*, 2008, **8**, 3364.